Arabian Journal of Geosciences (2022) 15:236
https://doi.org/10.1007/s12517-022-09545-x

ORIGINAL PAPER

Hydrological appraisal using multi-source rainfall data in PDM model over the Qinhuai River basin in China

Basile A. Akpovi[1] · Dehua Zhu[2] · Muhammad Ilyas Abro[2] · Agnidé Emmanuel Lawin[3] · Mendela Houngnibo[4] · Joseph Bessou[4]

Received: 12 July 2021 / Accepted: 13 January 2022

Abstract
The impacts of climate change are one of the challenges that the world is facing. This study evaluates the behavior of streamflows using various rainfall data in the Qinhuai River basin (China) through the probability distributed model (PDM) rainfall–runoff model. The methodology consisted of (i) assessing the hydrological model capability to reproduce the hydrological processes of the basin using multi-source rainfall and (ii) estimating present (2010:2015) and future (2020:2099) runoff using the regional climate model (RCM) under the representative concentration pathway's (RCP) scenarios 4.5 and 8.5; it must be noted that the downscaling and bias corrections are done by the China Meteorological Administration. The results are used for these works, (iii) trend analysis based on the Mann–Kendall methods. The results showed a decent performance of the model simulating streamflow over the Qinhuai River basin with 0.95 of R^2 for calibration and 0.77 for validation and a root-mean-square error (RMSE), respectively, of 29.7 and 86.25. The performance criteria of this model are determined through R^2 statistic and the RMSE. Rainfall data (rain gauge, C-band radar, S-band radar), Climate Prediction Center (CPC) morphing technique (CMORPH), and global precipitation measurement (GPM) satellite rainfall indicated fair adequation between the actual and simulated flows with statistic coefficient greater than 0.95 for calibration. A significant change trend at 0.05 level was found for the future runoff simulated under both RCP's scenarios at annual time scales.

Keywords Climate change · Hydrological modeling · Trend · Mann–Kendall · PDM · Qinhuai River basin

Introduction

Climate change across human activities has considerably affected and modified the hydrological cycles around the world. The natural disaster data (1980 to 2008) indicates that with 2887 flood events, over 2 billion people were affected, with 195,843 deaths, and had an approximated economic damage of more than US $X1,000) (Adediran 2015). The attraction of the widely distributed floodplains and the low-lying coasts to human settlement may explain the huge number of disasters observed worldwide. Climate change is expected to enhance the global hydrological cycles. Changes in precipitation will necessarily result in the modification of water balance components irrespective of the spatial scales (Oki and Kanae (2006).

Floods can occur anywhere after heavy rain. All flood plains are vulnerable, and heavy storms can cause flash flooding. Based on the number of disasters created by flooding, inundations, and water diseases, it is indispensable to

Responsible Editor: Broder J. Merkel

Muhammad Ilyas Abro is a co-first author.

Highlights
- Assessing the hydrological model capability to reproduce the hydrological processes of the basin using multi-source rainfall.
- Estimating present (2010:2015) and future (2020: 2099) runoff using the RCMs under the RCP's scenarios 4.5 and 8.5.
- The correlation coefficient is 0.95 for calibration and 0.77 for validation and has a RMSE, respectively, of 29.7 and 86.25.
- A significant change trends at 0.05 level found for the future runoff simulated under both RCP's scenarios at annual time scales.

✉ Basile A. Akpovi
assouanbasile01@gmail.com

✉ Muhammad Ilyas Abro
mohammadilyas.abro@yahoo.com

Extended author information available on the last page of the article

Published online: 24 January 2022

develop hydrological models, to manage and monitor the hydrologic system. Most of the population is living within 60 km, and it may be expected by 2010 that around 80% of the world population will be within 100 km near the ocean or major rivers (Adediran 2015). The hydrological processes include infiltration, groundwater recharge, and runoff which causes unbalance of water resources' demand, supply, and quality, thereby causing imbalances in the environment, ecosystems, and economy at large; the direct consequences of land-use change are the increasing rate of flood incidences, base-flow, and annual mean discharge, whereas the variability of climate can alter the peak flows, flow routing time, and volume (Ali et al. 2018). Similarly, climate change may alter the water cycle at various scales as depicted in the literature (Tolika 2019; Maraun 2016; Fang et al. 2015; Vrac et al. 2016; Rica 2020). Evaluating the impacts of climate change on hydrologic components is therefore necessary. Qinhuai River is strongly subjected to urbanization due to which an increased hydraulic efficiency decreases the capacity of moisture storage, leading to an increase in surface runoff (Bian et al. 2017). However, estimating the influence of climate change on the hydrological cycle is beyond the scope of this study.

Rainfall data availability is important in the hydrological models and the usefulness for the quality and management of water, flood forecasting, drought monitoring, etc. Different satellite rainfall estimation performs well in different region areas in the context of hydrological used, which is very crucial in appreciating the suitability of precipitation estimation in a given region. Based on the inconsistency of satellite rainfall estimation through different algorithms, rainfall data estimation needs to be confronted against in situ data and established the performance of it in the context of hydrological models. To achieve this control, hydrological model needs to be set. The validation of satellite data can be organized into three classes (Abro et al. 2019). For this study, it is a question to estimate the multi-source rainfall through hydrological modeling; simulate runoff used series of satellites (CMORPH, GPM) and radars (S-band radar, C-band radar) based on rainfall products; make a prediction of flow over the long-term under RCP's scenarios; and evaluate the effect of climate change in this basin. For doing well this work, we need the DEM to make catchment area, the meteorological data (rain gauges), the hydrological data(flows), and satellite data. ArcGIS software is used for delineating hydrology basin, the probability distributed model rainfall (PDM) runoff is used for simulation flow, and the representative concentration pathway (RCP) is used for the long-term prediction about hydrological climate change on this river.

The present study aims to evaluate multi-source rainfall through hydrological model PDM and appreciate the impact of climate change on the Qinhuai River basin. The novelty of the present study is to construct the surrogate of the Qinhuai River basin catchment so that the catchment hydrological behavior would be represented by the hydrological model PDM. The other scope and novelty of this study are to examine the performance of the suggested methods by multiple criteria (statistical and hydrographs) for confirming the precision of the produced hydrological results from the different remote sensing data. The last scope is to analyze the behavior of flow simulation through PDM in the future under the RCP's 4.5 and 8.5 scenarios using MK methods analysis. Very limited or no study has been found for this catchment which has used RCP's for trend detection.

Study area

Qinhuai River is the tributary of the lower Yangtze River, and it is located in 118°39′ to 119°19′ E longitude and 31°34′ to 32°10′ N latitude; its elevation varies between 0 and 41 7 m above sea level. The watershed area is about 2642.98 km^2. The main Qinhuai River flows 110 km across the urban area of Nanjing before joining the Yangtze River (Song et al. 2015). The studied basin lies in the humid climatic region; the annual mean temperature is 15.4 °C, the annual precipitation is 1116 mm (1986–2013), and the rainy season extends from April to October. According to Hao et al. (2015), June to August monsoon rainfall causes flood in this catchment which contributes the major annual runoff (430 mm). Since the beginning of the twenty first century, the urbanization has started in this basin due to which land-use has changed in the Qinhuai River basin. So, the hydrological process and other related process changes were obvious. Therefore, it is most important to find out the impacts of land-use change and hydrological response. Figure 1 represents the study area and locations of rain gauges and flow gauge.

Data and methods

Data

We considered the climate data and the satellite and radar products in this study. To recognize the influence of precipitation inputs on the hydrological model, the correctness of the precipitation of satellite and S-band radar was first evaluated against the rain gauge precipitation. So, the satellite data and radar's data were evaluated against basin average (rain gauge). Thus, we compared the satellites data and radar's data against the rain gauge observations for the period 1 July 2014 to 21 July 2015. Each of these datasets we used is described below.

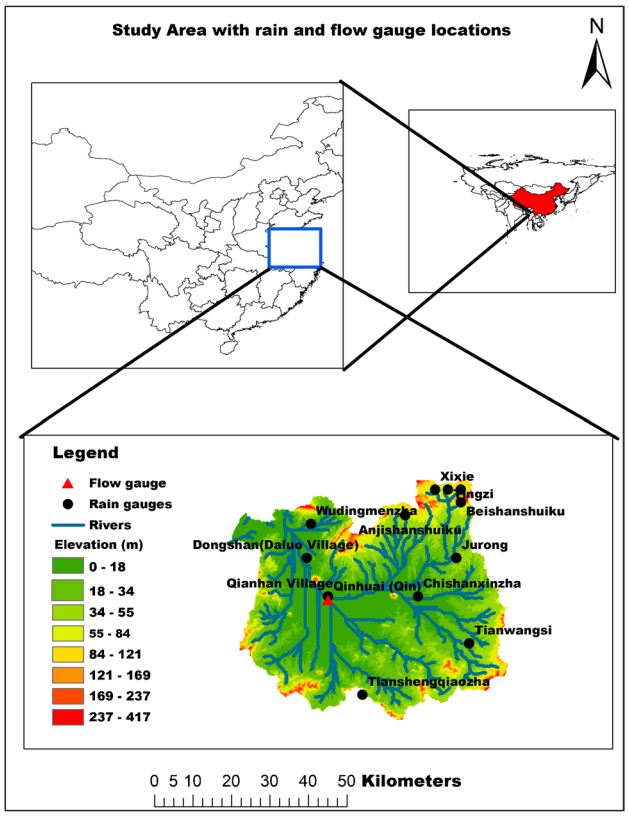

Fig. 1 The Qinhuai River basin and the locations of hydrometeorological stations

Climate data

Hourly precipitation from 2010 to 2015 was obtained from the China Meteorological Administration for the selective 12 automatic meteorological stations. The daily runoff data are provided by the China hydrological services. The locations of rain gauge stations are shown in Fig. 1. These stations were selected due to the availability of data during the study period. The rain gauges have the ability to measure both liquid and solid precipitation for around the day, and then it was converted into accumulated precipitation at 8 pm local time every day. The quality check has been performed by the National Meteorological Information Center (NMIC).

The future climate data (rainfall and potential evaporation) for the period from 2020 to 2099 under RCP scenarios 4.5 and 8.5 are provided by the China Meteorological Administration. The global climate model data used is the European Centre Hamburg Model (global climate model) ECHAM5, downscaling in the regional model RegCM4.0 with 50 km horizontal resolution and 18 vertical levels. The bias correction of model output comes from this study (Zhu et al. 2017).

Satellites and radar products

CMORPH and GPM Mission are the two satellite precipitation products evaluated in this study. The National Oceanic and Atmospheric Administration (NOAA) through the Climate Prediction Center's MORPHing technique have produced CMORPH. Nowadays, its reprocess product is available. The CMORPH-GC has 0.1° spatial resolution and 1 h of temporal resolution. Its coverage is 70°W to 140°E and 15°S to 44°N and produces hourly precipitations. We downloaded the data from 2010 to 2015 at http://www.ftp.cpc.ncep.noaa.gov/precip/ (accessed on 17/07/2018).

The GPM mission is a collaborative effort by the National Aeronautics and Space Administration (NASA) and the Japan Aerospace Exploration Agency (JAXA), which provides precipitation estimates around the globe. It has spatiotemporal 0.1° and temporal 30 min resolution with coverage from 60°N to 60°S. The data was downloaded from 2010 to 2015 at https://pmm.nasa.gov/data-access/downloads/gpm (accessed on 17/07/2018).

Rainfall radars C-band and S-band are used in this study. The radar C-band has 0.5°/75 m of spatial resolution and 6 min of temporal resolution with a 250 km radius of coverage. As for the radar S-band, it has 1°/250 m of spatial resolution and 6 min of temporal resolution with a 250 km radius of coverage. The respective data were taken from Nanjing University of Information Science and Technology and the China Meteorological Administration.

Methods

All the data have been collected/downloaded from their respective sources. The Thiessen polygon method has been used to find out the weight for all rain gauges in the study area. Furthermore, the average values for study area have been calculated with the help of MATLAB for all satellite and reanalysis data sources. After that, the hydrological model (probability distributed model (PDM)) has been calibrated and validated with the selected events, and then the model was run for actual event analysis. Moreover, the simulated runoff under RCP's scenarios (4.5 and 8.5) has been tested for the trend analysis using sequential Mann–Kendall for temporal scales of the annual, decadal, seasonal, and monthly average. More details about the methods are in the next section.

Thiessen polygon method

The spatial average of rainfall over the study area was appraised using the Thiessen polygon method which assigns weight to each gauge station proportionally to the catchment area the station covers. The surface area (A_i) of the influence zone of the station (refer here as sub-catchment)

is divided by the total catchment area (A) to obtain the rain gauge weight W_i:

$$W_i = \frac{A_i}{A}, \tag{1}$$

The spatial average rainfall of the catchment area is computed as

$$P = \sum W_i P_i, \tag{2}$$

where P_i is rainfall at the point scale for each sub-catchment area.

Probability distributed model (PDM)

Several hydrological models have been used in China (SWAT, Du et al. (2013) and HEC-HMS, Oleyiblo and Li (2010) and Liuxihe (LXH) model (Zhu et al. 2020)). However, the probability distributed model (Adediran 2015) has not been widely used, and this justified its selection in this study. PDM is a lumped rainfall–runoff model which works on the probability distributed moisture stores and translation of runoff and drainage via routing stores (Moore 2007). Its structuration is shown in Fig. 2.

The probability distributed store is the source for direct runoff, groundwater recharge, and soil moisture storage. Flow routing systems can be defined by a variety of nonlinear storage reservoirs or by a cascade of two linear reservoirs. The choice of nonlinear storage includes linear and quadratic storages along with exponential, cubic, and general nonlinear forms. A cubic form represents groundwater storage.

The equations that govern the flow estimating are computed as

$$q = kS^3, \tag{3}$$

where q is flow discharge and S is the basin capacity (m^2). An estimated solution using the Smith (1977) method to give out the following recursive equation which can be used for storage, for constant input u over the interval $(t, t+\Delta t)$, is as follows:

$$S(t+\Delta t) = S(t) - \frac{1}{3kS^2}\left(exp\left(-3kS^2(t)\Delta t\right) - 1\right)\left(u - kS^3(t)\right), \tag{4}$$

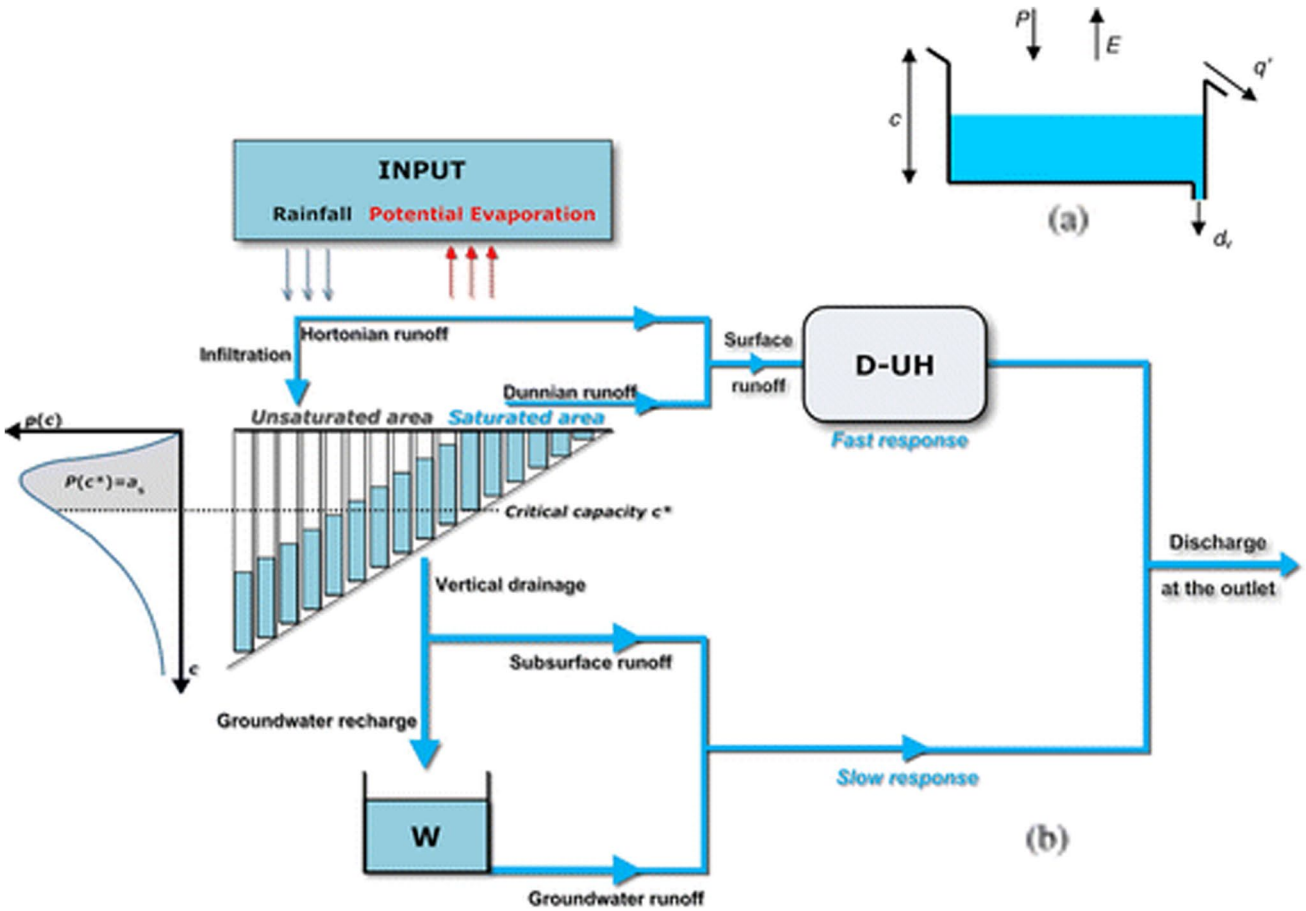

Fig. 2 Probability distributed model rainfall–runoff (Moore 1985, 1999, 2007)

From this equation, the discharge is obtained through the nonlinear relation:

$$q(t+\Delta t) = kS^3(t+\Delta t) \tag{5}$$

The surface storage is a combination of two (2) linear reservoirs; they have time constants k_1 and k_2, with separately coincident transfer function model (O'Connor 1982):

$$q_t = -\delta_1 q_{t-1} - \delta_2 qt - 2w_0 u_t + w_1 u_{t-1}, \text{with} \tag{6}$$

$$\delta_1 = -(\delta_1^* + \delta_2^*), \delta_2 = \delta_1^* \delta_2^*, \delta_1^* = exp(-\Delta t/k_1), \delta_1^* = exp\left(-\frac{\Delta t}{k_2}\right) \tag{7}$$

$$w_0 = \frac{k_1(\delta_1^* - 1) - k_2(\delta_2^* - 1)}{k_2 - k_1}, k_1 \# k_2 \text{ and } k_0 = 1 - (1 + \Delta t/k_1)\delta_1^* \tag{8}$$

$$w_1 = \frac{k_1(\delta_2^* - 1)\delta_1^* - k_1(\delta_1^* - 1)\delta_2^*}{k_2 - k_1}, k_1 \# k_2 \text{ and } w_1 = (\delta_1^* - 1 + \Delta t/k_1)\delta_1^* \tag{9}$$

It is expected that input u_1 remains constant over this interval Δt (between t-1 and t). In this case, the input is the volume of direct runoff, V(t), and the output q_t will be the surface flow component of the total basin runoff, $q_s(t)$. S(t) is the store of the basin. There are 13 parameters in total used for PDM.

Model calibration process

Both automatic optimization and visually interactive parameter estimation have been done within the generic model calibration shell environment. The simplex direct search procedure for automatic optimization was given by Nelder and Mead (1965), later amended by Gill et al. (1981), and an interactive visualization tool was used to find out the impact of parameter changing over the shape of hydrograph. Furthermore, this calibration environment is responsible for the mean and peak error statistical indicators for actual and simulated flow. The objective function is used for surface analysis of parameter dependency on one another (Moore 2007). Both the manual and automatic parameter adjustment have been utilized for observing the best fit between actual and simulated flow.

Model calibration matric

The model calibration has been done using the rain gauge data from 2010 to 2011. The model provides many measures of model performances which are R^2 coefficient and root-mean-square error (RMSE). The quantitative examination of the model has been done through correlation coefficient R^2 that represents the agreement between actual and simulated flow, and the RMSE was used to find out the differences in the magnitude of peaks.

Both statistical indicators were used by many researchers (Nkunzimana et al. 2019; Abro et al. 2020b; Zhu et al. 2020).

Mathematically defined as

$$RMSE = \sqrt{(n^{-1}\sum e_t^2)}, \tag{10}$$

$$R^2 = 1 - \frac{\sum e_t^2}{\sum (Q_t - \overline{Q})^2}, \tag{11}$$

$$\text{with } e_t = Q_t - q_t, \tag{12}$$

e_t is the model error, Q_t is the observed flow at time t, q_t is the computed flow, and $\overline{Q}$ is the mean of the observed flow.

Model validation

After running the model, if the value of R^2 is not too close to 1 like 0.6–0.9, because the area catchment and the scale of variation of the observations within each period depend on it also, we have to set the model parameters and run the model again with new input data. For this validation, we use the data from 2012 to 2015. The model is validated when RMSE is closed to 0 and R^2 close to 1. So we conclude that the model fits well with the observed data.

Mann–Kendall method

The Mann–Kendall non-parametric test (Mann 1945; Kendall 1975) is largely used worldwide for hydrologic data analysis. In Benin, Agnidé Emmanuel Lawin 1, 2,*, Nina Rholan Hounguè 2, Chabi Angelbert Biaou 3, and Djigbo Félicien Badou 1, 2 used this method analysis in the current and mid-century trends in rainfalls and temperature over the Mono River watershed. In Burundi, the Mann–Kendall methods (Niyongendako et al. 2020) were used to detect extreme climate change in this country. It is used to detect trends that are monotonic but not necessarily linear (Sridhar and Raviraj 2017). The MK test is based on a null hypothesis that indicates there is no trend in the data and it is random and independent which is verified against the hypothesis which supposes there is a trend in the data (Bengal 2014).

The Mann–Kendall test statistic S is calculated using the formula as follows:

$$S = \sum_{i=1}^{N-1} \sum_{j=i+1}^{N} sgn(x_i - x_j) \tag{13}$$

with x_i and x_j are the annual values in years j and i, j > i respectively, and N is the number of data points.

The sequential version of Mann–Kendall (SMK) test statistic (Sneyres 1990) on time series x_i detects the recognized event or change points in long-term time series. The sequential Mann–Kendall test is computed using ranked values, iy of the original values in analysis $(x_1,x_2,x_3,..,x_n)$. The magnitudes $(i=1, 2,3,\ldots, n)$ of y_i are compared with magnitudes of y_j, (1, 2,3,…, i -1).

The only comparison that was counted was $> y_i y_j$, and it is denoted by n_i. The statistic t_i can be defined as

$$t_i = \sum_{j=1}^{i} n_i \tag{14}$$

The distribution of test statistics t_i has a mean as

$$\mathrm{E}(t_i) = \frac{i(i-1)}{4} \tag{15}$$

The sequential values of a reduced or standardized variable, called statistic $u(t_i)$, is calculated for each of the test statistic variables t_i as follows:

$$u\left(t_i\right) = \frac{[t_i - E(i)]}{\sqrt{var(t_i)}} \tag{16}$$

While the forward sequential statistic (t_i) is estimated using the original time series $(x_1,x_2,x_3,..,x_n)$, values of the backward sequential statistic, $(u^{'}(t_i)\ t$, are estimated in the same manner but starting from the end of the series. In estimating $(u^{'}(t_i)$, the time series has resorted so that the last value of the original time series comes first $(x_1,x_2,x_3,..,x_n)$. The sequential version of Mann–Kendall test statistic allows detection of the approximate beginning of a developing trend. When $(u(t_i)$ and $(u^{'}(t_i)$ curves are plotted, the intersection of the curves $(u(t_i)$ and $(u^{'}(t_i)$ locates approximate potential trend turning points. If the intersection of $(u(t_i)$ and $(u(i)$ occur beyond ± 1.96 (at the significance level $\alpha = 5\%$) of the standardized statistic, a detectable change at that point in the time series can be inferred.

After the calibration has been performed, then the model was driven with RCM historic data to find out its suitability; once it is up to mark, then it will be driven by the RCM with two emission scenarios (RCP4.5 and RCP8.5) to produce multiple runoff simulations. The RCM-based daily climate simulations were expected to capture the changes in daily climate variables that are directly related to the analysis of extreme events relating to daily precipitation intensity and flood frequency on the catchment (Fig. 3).

Results

Calibration and validation of model

The overall performance of the PDM model is represented by R^2 and RMSE values of 0.95 and 29.70 $m^3.s^{-1}$ for the calibration and 0.77 and 86.25 $m^3.s^{-1}$ during the validation

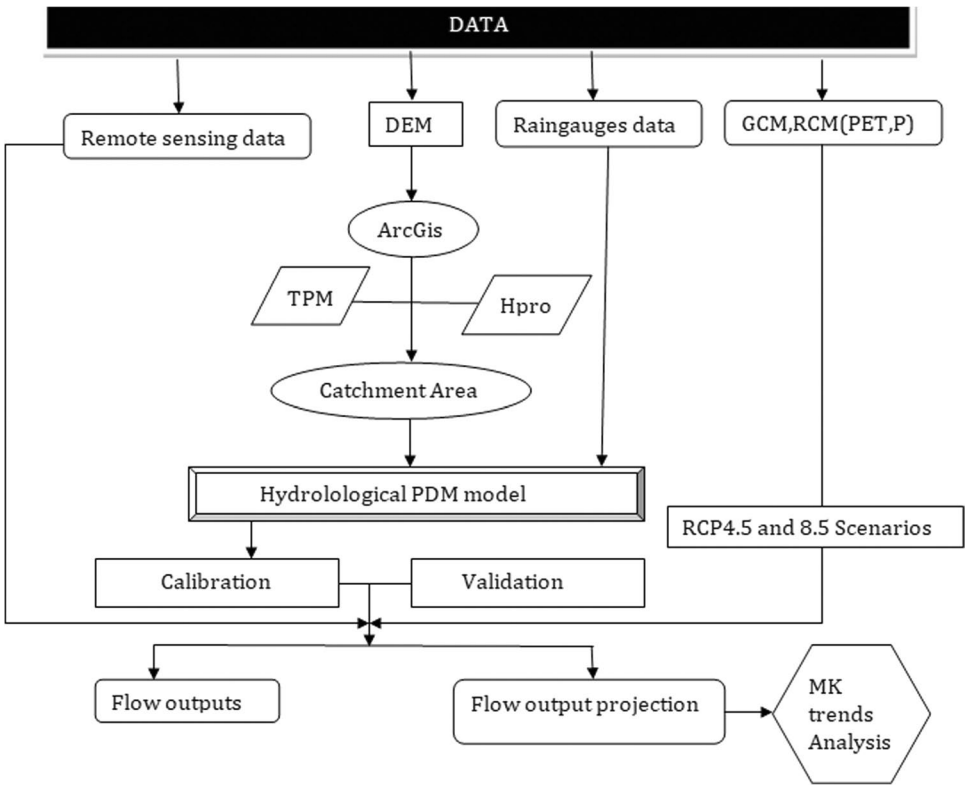

Fig. 3 A summarized procedure of the study

for Qinhuai River basin (QRB), respectively; similar results for calibration and validation have been found by Abro et al. (2020a) using PDM over Gilgit Basin in Pakistan. Abro et al. (2021) have simulated multi-sources for hydrological purposes over the Huaihe River basin in China which used PDM and found that the coefficient of determination for calibration and validation were 0.83 and 0.68 and RMSE for calibration and validation 12.76 and 18.74. respectively. The calibrated and validated hydrographs are shown in Fig. 4. The modeling results tend to match the observed flow well, while there is an overestimation of all peaks of flows for QRB during the calibration that was observed. Contrary, this overestimation is a little higher for the validation period. Despite of overestimation, during most of the flow events, the PDM has a good performance, and all correlation (R^2) values are sufficiently high for an acceptable hydrological model.

Response of different rainfall data simulation with PDM

The performance of multi-sources of rainfall products for three events through PDM hydrological model was assessed, by comparing the simulated streamflow driven by rain gauge measurements, CMORPH and GPM satellites, and C-band and S-band radar rainfall data.

Flood event 1

Each rainfall data has been used to compute flow through PDM model for each hour, over July 01–08, for observed flows and simulated flows using observed rainfalls, C-band radar, S-band radar, CMORPH, and GPM rainfalls. The results (Figs. 5 and 6) were shown by using the observed and multi-source rainfalls; it showed few differences among observed and simulated hourly flow. The flows simulated with different rainfall data range in the same way with the observed flow. For the rain gauge, the statistic coefficient R^2 is 0.99, and the RMSE is 16.21 m^3s^{-1} of simulated flows in comparison with the observed flows. For C-band radar, the R^2 and RMSE are 0.99 and 16.21 $m^3.s^{-1}$, respectively, while for S-band radar, the R^2 and RMSE are, respectively, 0.98 and 29.99 $m^3.s^{-1}$. The R^2 and RMSE, respectively, for CMORPH and GPM satellites are 0.98, 23.60 $m^3.s^{-1}$, and 0.98, 23.08 $m^3.s^{-1}$. These results are illustrated in Fig. 5 (event 1). It can be remarked that the C-band radar had a lower RMSE, and GPM satellite, S-band radar, and CMORPH satellite had lower R^2, while S-band radar had higher RMSE, and the C-band radar has higher R^2. The performance of all data sources (satellite and radar) looks decent based on the criterion. Amorim et al. (2020) have studied over Tocantins-Araguaia river basin (TARB), Brazil, throughout June 2000 to December 2018 and used soil and water assessment tool (SWAT). They have found calibration 0.82 and validation value 0.83 for GPM (IMERG), which are comparable to this study.

We remarked also that the model overestimates the rising of the flow (Fig. 6).

Flood event 2

The simulation results with PDM using different rainfalls data reveal reasonable outcomes when comparing observed and simulated flows, as demonstrated in Figs. 3 and 4. In addition, to discuss the discharges, this study, from the 2nd of July to the 6th of June in that period, extreme rainfall occurred. Figure 7 and 8 show simulated flow peaks which are in resemblance to observations. The R^2 values are 0.98, 0.98, 0.97, 0.99, and 0.98, respectively, for the rain gauge, C-band radar, S-band radar, CMORPH, and GPM. There is a good correlation between simulated and observed results. In addition, the value for RMSE is around 32.28, 24.18, 36.08, 22.35, and 26.04 $m^3.s^{-1}$, respectively. The CMORPH satellite had the lowest RMSE, and the S-band radar had the lowest R^2, while S-band radar have the highest RMSE, and the CMORPH satellite had the highest R^2.

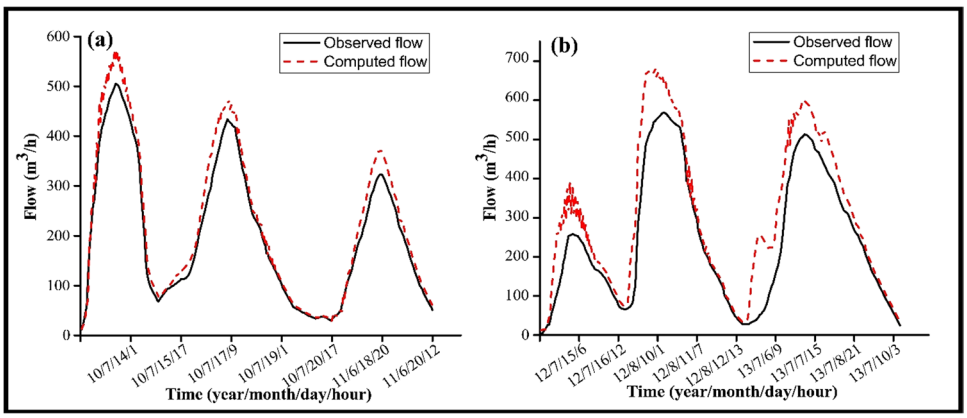

Fig. 4 The calibration (**a**) and validation (**b**) hydrographs generated by PDM model in QRB

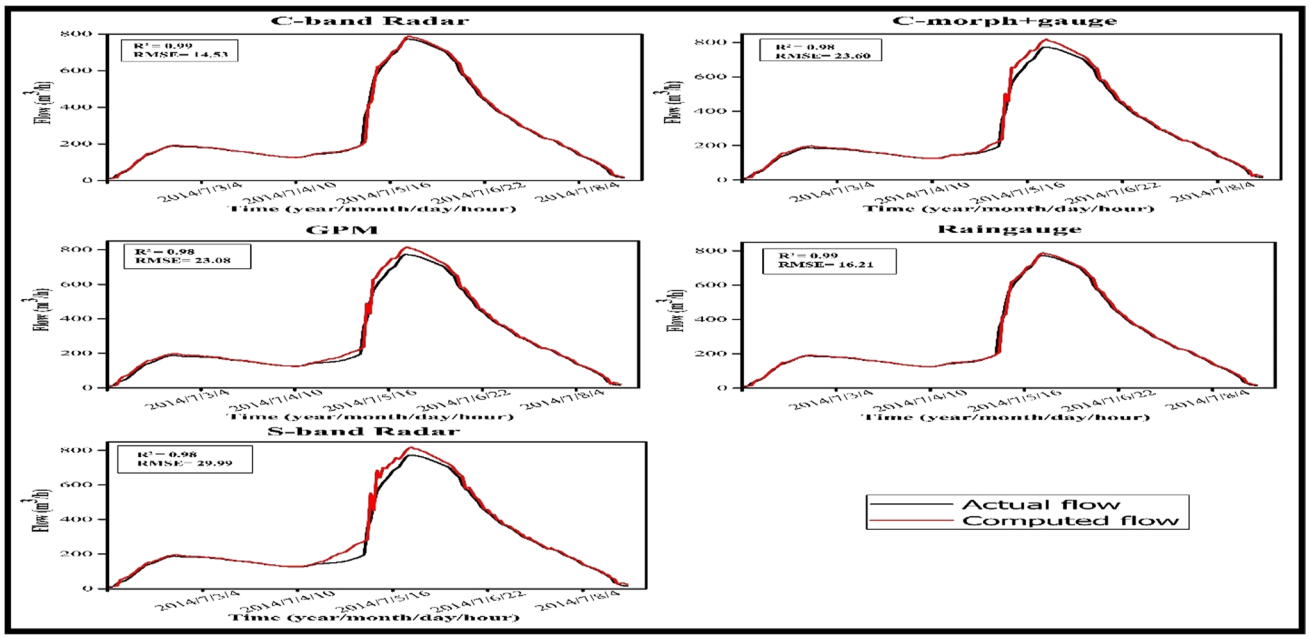

Fig. 5 Observed and simulated discharge (flood event of July 2014) with the different rainfall sources

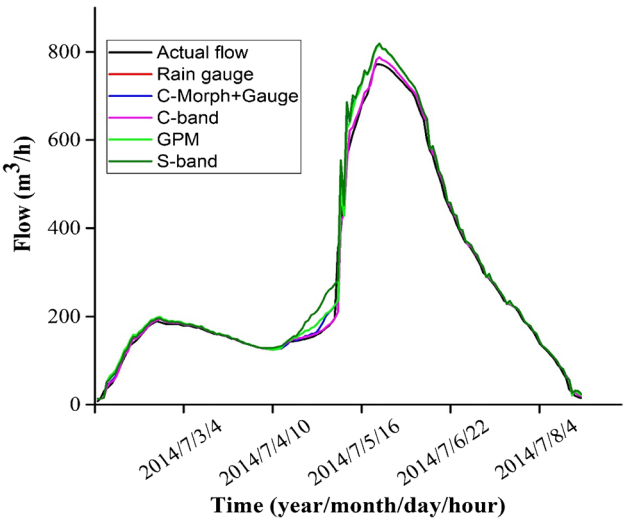

Fig. 6 Combined comparison of observed and simulated discharges with different satellites and radar rainfall data

Comparatively of the observed data, all rainfall estimated by remote sensing used in this study overestimated lightly the pick of the flow simulation.

Flood event 3

For the third flood event, the simulated flow compared to the observed flow reveals a good agreement as shown in Figs. 9 and 10. The different rainfall data perform well through the model, and the relationship between observed and flow simulated is excellent. The different coefficients are 0.99, 0.99, 0.98, and 0.97, respectively, for the rain gauge, C-band radar, S-band radar, CMORPH, and GPM satellites, and the RMSE are, respectively, 24.85, 24.36, 35.72, 24.17, and 45.50 $m^3.s^{-1}$. The CMORPH satellite had the lowest RMSE, and the GPM satellite had the lowest R^2, while GPM satellite had the highest RMSE and CMORPH satellite, and C-band radar had the highest R^2 (Fig. 9 (event 3)). It was observed that the model overestimated the rising flow in opposition to the recession part of the hygrograph which was well represented (Fig. 10).

Evolution of runoff simulation under climate change

To better appreciate the climate change influence on runoff in Qinhuai river basin, we simulate the runoff under RCP's scenarios (4.5 and 8.5). The hydrological practices in the study area were simulated with the calibrated PDM model, using input rainfall and potential evaporation from the GCMs (ECHAM5) and RCM for the period 2020–2099. Decadal runoff simulation under RCP's scenarios is analyzed using SMK test statistics. The results of SMK test statistic for decadal data set of runoff simulation under the RCP's scenario showed clearly the detection of the statistical significant change point in decadal trends of runoff (Fig. 11a–b). From the first to the eighth decade, we observed the detected point of change in the end of the first decade, beginning of the second decade, the beginning of fourth decade, the end of the sixth, and beginning of seventh decade. We observed the increase of the trend at the

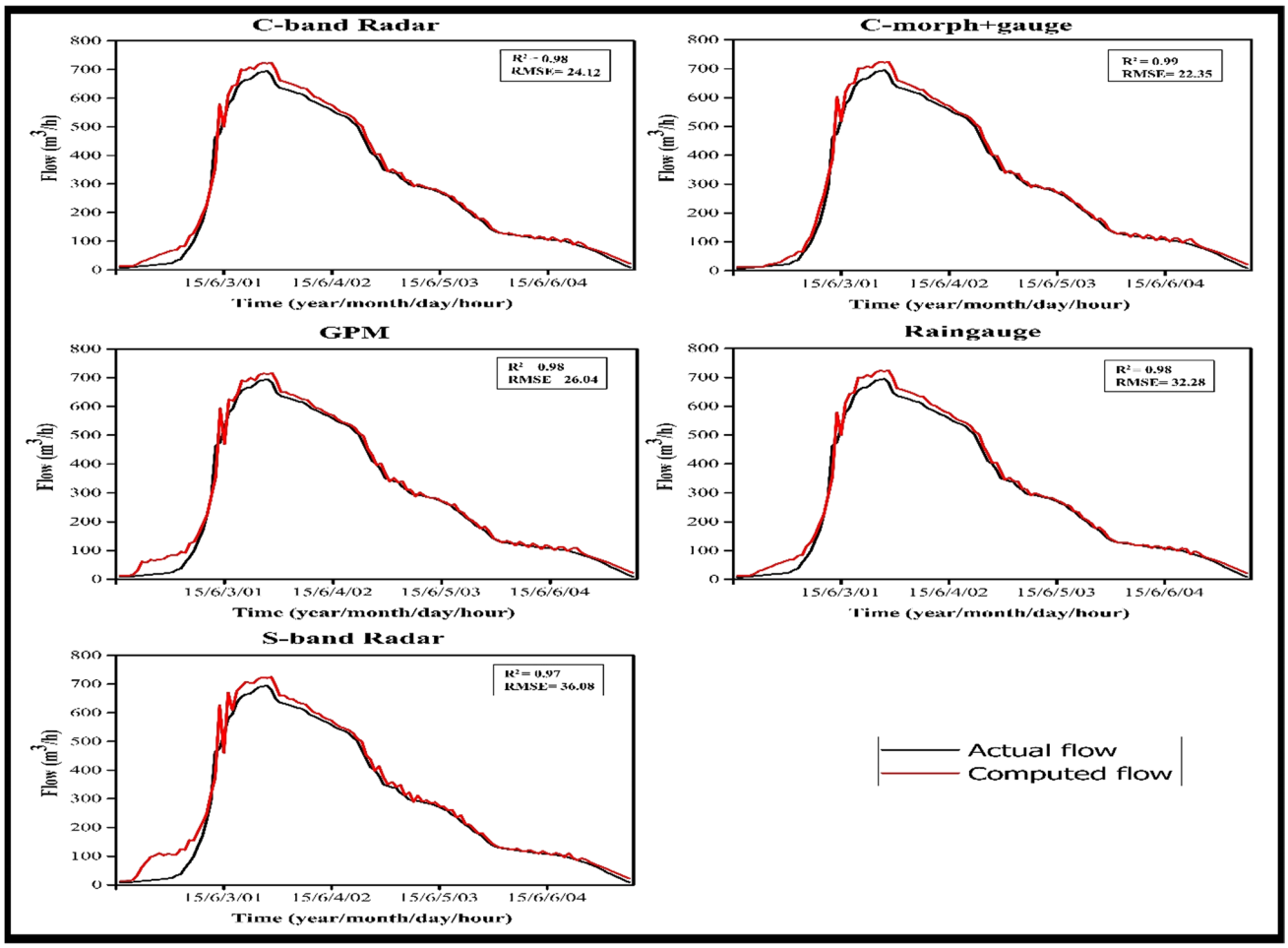

Fig. 7 Flood event 2 corresponding to June 2015

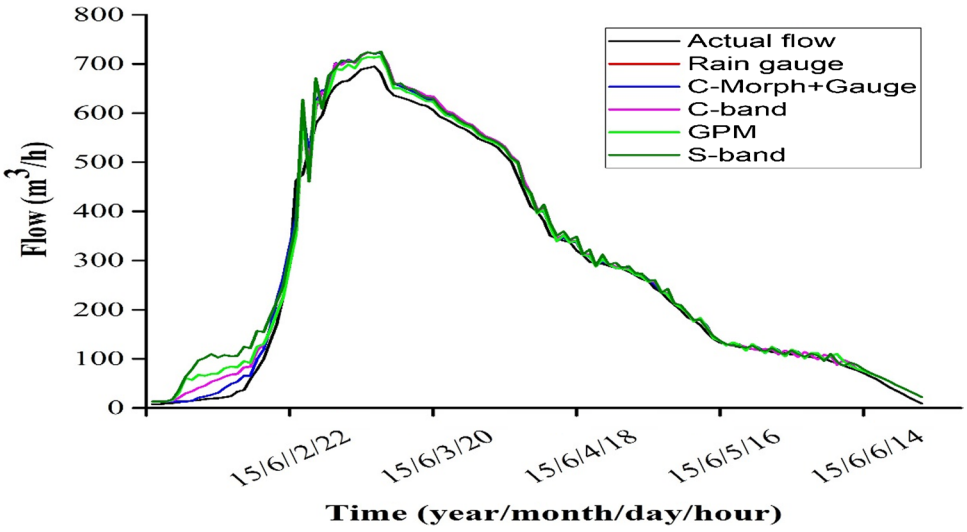

Fig. 8 Combined comparison of observed and simulated discharges with different satellites and radar rainfall data (June 2015 flood event)

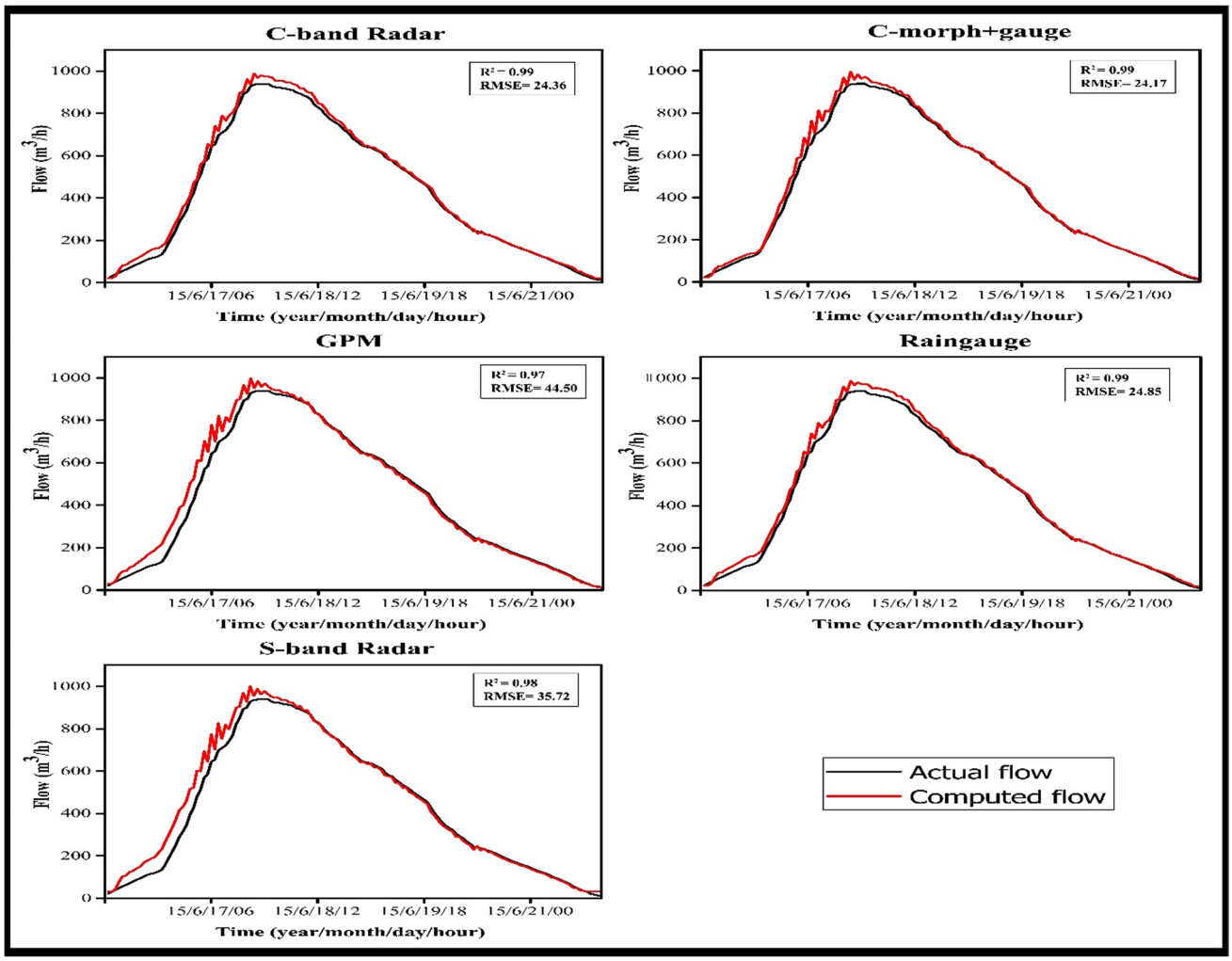

Fig. 9 Flood event of July 2015

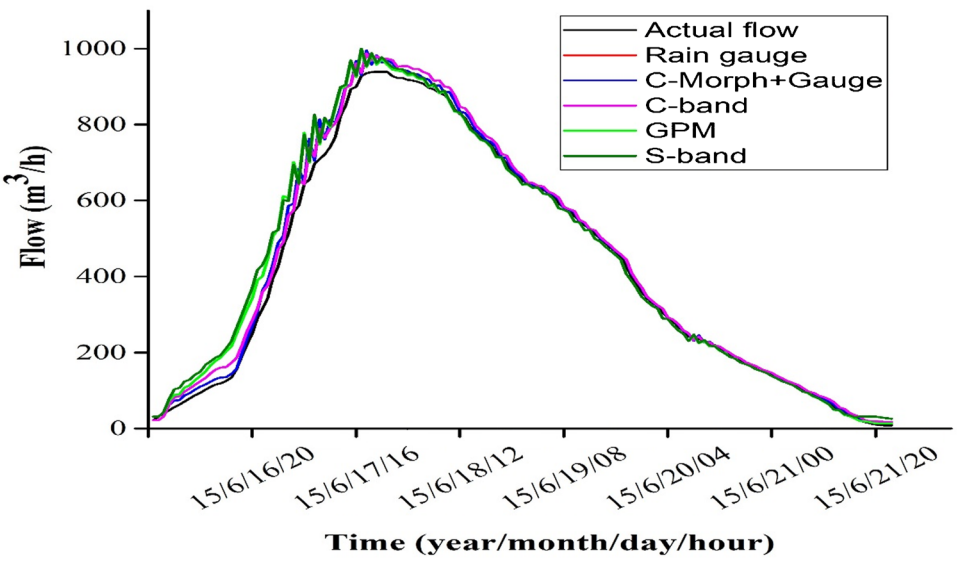

Fig. 10 Combined comparison of observed and simulated discharges with different satellites and radar rainfall data (July 2015 event flood)

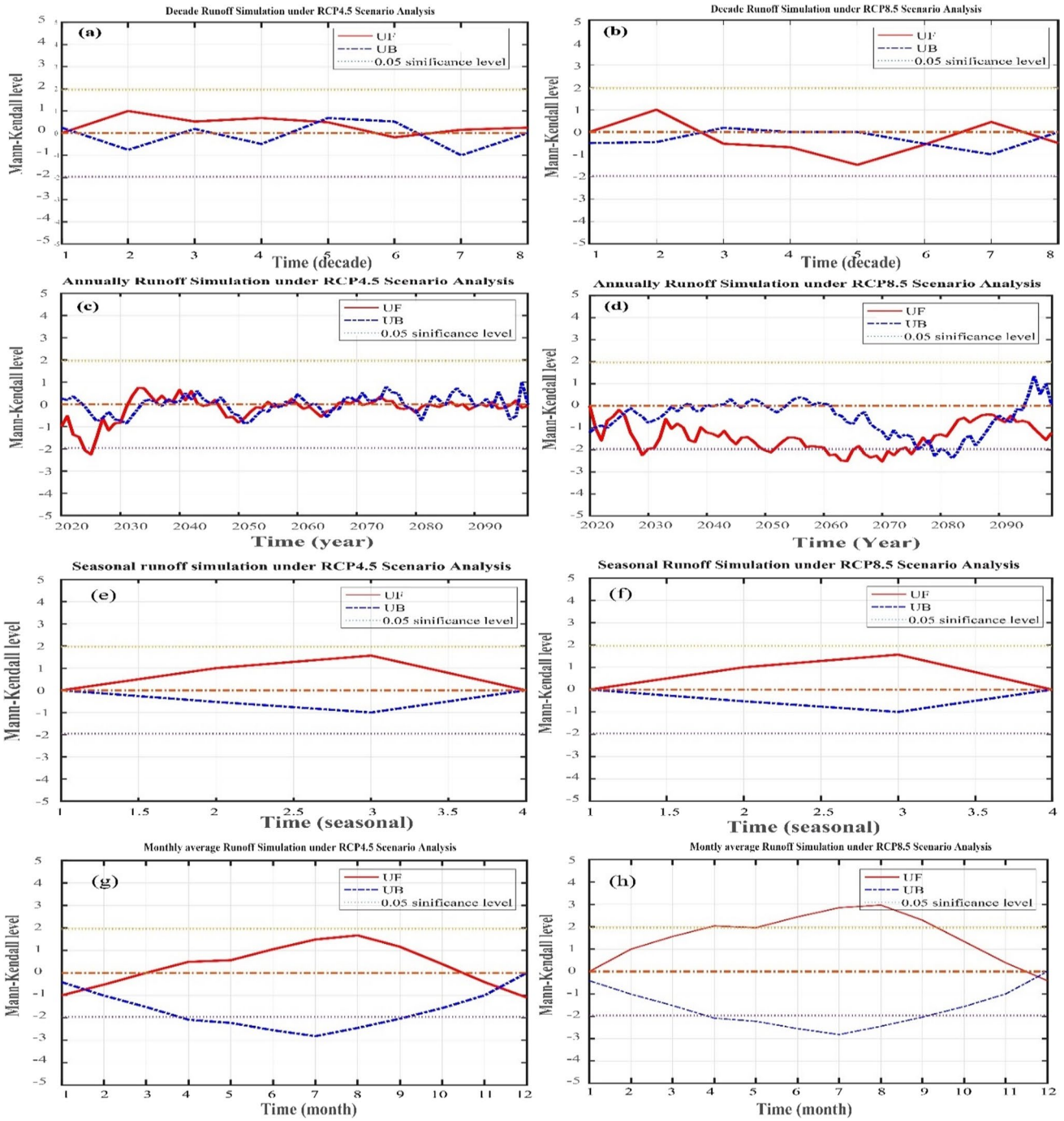

Fig. 11 The abrupt change in average decadal (**a**-**b**), yearly (**c**-**d**), seasonal (**e**-**f**) and monthly (**g**-**h**) runoff simulation trends under RCP's scenarios as resulting from SMK test statistic

beginning of the second decade and fourth and seventh for the backward sequential curve (Fig. 11a). The decreasing of the trend is observed with the forward sequential curve during the same time. The same observed is noted under the RCP8.5 scenario, but at the beginning of the second decade, we observed an increasing of the backward sequential curve and the decreasing of the forward sequential curve until the fifth decade and from the beginning of the fifth decade until the change point at the end of sixth decade, but the decreasing of forward curve is observed at the beginning of seventh decade (Fig. 11b).

The trend simulation analysis is submitted of sequential Mann–Kendall test statistic for annually, decadal, seasonal, and monthly average.

Yearly plots of Uf and Ub have been shown in Fig. 11. Under RCP4.5 scenario, a decreasing trend from 2020 to 2026 is observed. The forward and backward trends were intercepted several times where we observed the significant turning point due to a probability value less than the accepted level of significance ($p \leq 0.05$). From 2031, where we observed the significant detecting point of trend change, we notified a continuous increasing trend until 2042. From this year, the curves of Uf and Ub show a decreasing trend until 2051 where both of them intercepted with a significant change. The trends started increasing till 2060 where another significant detected point is observed. From this significant point to 2066 where both of the curves were intercepted, we have decreasing trends. In 2073, the forward and backward curved intercepted, we observed an decreasing trend until 2080. From 2080, we note several detecting change points, but the increasing or decreasing trends is not so pronounced (Fig. 11c). Under the scenario RCP8.5, the runoff simulation for annual average plot reveals the significant detecting point trend changes in 2077. From this significant point, we observed an increasing trend till 2088 (Fig. 11d).

The seasonal runoff simulation under the RCP's scenario showed the detection point of change at the beginning and end of the season. In the beginning, we observed the increasing of the forward sequential curve and the decreasing of the backward curve, and in the end, it's the opposite (Fig. 11e–f). The same observation is remarked with the monthly average runoff under the RCP's scenarios (Fig. 11g–h).

Under the RCP4.5 scenario, the Mann–Kendall analysis statistics of monthly average flow long-term simulation (Fig. 11g) showed an increase in long-term flow prediction from January to August and gradually decreasing trend from August to December. The forward and backward sequential statistics intersected around February and December which form periods of trend change, which indicate the periods in which change took place. The forward and backward sequential statistics UF and UB intersected the significant confidence level trend $UL = -1.96$ during the months April and October. That means there is a significant decreasing change of trend flow during this period of prediction flow under the RCP4.5 scenario. The RCP8.5 showed also an increasing trend in the long-term flow prediction from January to August and gradually decreasing trend from August to December (Fig. 11h). The forward and backward sequential statistics intersected around December which forms periods of trend change, which indicate periods in which change took place. The forward and backward sequential statistics UF and UB intersected the significant confidence level trend $UL = -1.96$ and $UL = 1.96$ during the months March to April and October. That means there is a significant decreasing and increasing change trend of monthly average flow during this period of prediction flow.

Discussion and conclusion

Satellite rainfall estimation is indispensable for monitoring and forecasting at the national, regional, and global levels in the water resource management and policies makers. Satellite precipitation products offer new varieties of input data with high resolution (i.e., continuous, remote, mountainous, and transboundary basins).

This study aims to discover the potential of satellite, radar and reanalysis precipitation, and flow estimates during the study period (2010–2015) at the catchment level and evaluate future flow simulation under RCP's 4.5 and 8.5 scenarios. To evaluate the performance of remote sensing rainfall in terms of rainfall estimation, we compared them with rain gauge measurements. Hydrological model was constructed in the Qinhuai River basin catchment. After calibration and validation of hydrological model, we simulated long-term runoff under climate change scenario RCP 4.5 and 8.5. Non-parametric Mann–Kendall methods were used to detect the abrupt change of flow simulation in the future.

The PDM model successfully calibrated, validated, and generated better simulation results (Fig. 4). The model reproduced a good flood hydrograph but overestimates the recession hydrograph. The evaluation of the model performance was carried out successfully with the available performance criteria with an R^2 value above 0.70 for calibration and validation. Multi-sources of rainfall data (rain gauge, C-band radar, S-band radar, CMORPH, and GPM satellite rainfall) are used for flow simulation. The observed flow and simulated flow correlated well with the R^2 greater than 0.95. The model indicates a satisfactory performance with the different rainfall input (Figs. 7, 8 and 9). Further analyses show that the investigated satellite products tend to show good performance when these products are used to predict flow relative to the observed rainfall over China especially over Qinhuai River basin (Huang et al. 2016). Based on the future climate change scenarios, future runoff data have been simulated using PDM model to evaluate the long-term variability of flows. The increasing trend in river levels has been observed through modeling by all climate scenarios (near future, future, and distant future). Many studies confirmed the increase of flood level in this catchment area of China (Gu et al. 2014). The runoff simulations under the RCP's scenarios using MK sequential Mann–Kendall test statistic trend analysis revealed some detection points of change, especially during 2026, 2031, 2042, etc. where yearly runoff trend change is mostly observed. We should notify that the increasing and decreasing runoff yearly trends under two scenario are frequently observed during the projection period (2020–2099). The same remark is also observed with the decadal runoff trend (Fig. 11a, b, c, d). But with the seasonal and monthly runoff trend simulation, two detection

points of change are observed in the beginning and the end of the trend where increasing and decreasing forward and backward curves of MK are noted.

Using climate and hydrological models for runoff simulation is a good step toward understanding, monitoring, and predicting floods. This methodology was adopted using local-scale and regional and global models to predict flood under climatic scenario conditions. PDM rainfall–runoff catchment simulation model has been calibrated and validated for Qinhuai River basin, for the prediction of its hydrologic response. The analyses have been done on graphical and statistical basis, and it was observed that R^2 was above 0.70 for calibration and validation, respectively. Multisource of rainfall data (rain gauge, C-band radar, S-band radar, CMORPH, and GPM satellite rainfall) used for flow simulation a fair adequation among actual and simulated flows with the statistic coefficient greater than 0.95. The model indicates a satisfactory performance with the different rainfall data. The model performance for calibration and validation and analyzed events was acceptable for all input sources. The model was successfully calibrated and validated and produced good runoff simulation.

This study allows detecting the potential of satellite-based precipitation estimates for flood forecasting at the catchment level. The statistical evaluation of rainfall is through GPM, CMORPH, C-band radar, and S-band radar and evaluated their utility for streamflow prediction using the PDM model in the Qinhuai River Basin, Nanjing, China. The major innovation of this paper are as follows:

(1) Evaluate the performance of satellite rainfall in terms of rainfall estimation and construct hydrological models in the Qinhuai Basin river catchment.
(2) The hydrological model was calibrated and validated with the rain gauge measurement, and hydrological behavior was studied in this catchment.
(3) The model was used to test the different rainfall inputs and compare the simulated streamflows with the measured recorded.
(4) The impact of climate change on the catchment in the future (2020–2100) was studied under the RCP's scenario through the PDM model streamflow simulations.

Declarations

Conflict of interest The authors declare no competing interests.

References

Abro MI et al (2019) Hydrological appraisal of rainfall estimates from radar, satellite, rain gauge and satellite–gauge combination on the Qinhuai River Basin, China. Hydrol Sci J 64(16):1957–1971. https://doi.org/10.1080/02626667.2018.1557335

Abro MI et al (2020a) Hydrological evaluation of satellite and reanalysis precipitation products in the glacier-fed river basin (Gilgit). Arab J Geosci 13(14):631. https://doi.org/10.1007/s12517-020-05621-2

Abro MI et al (2020b) Statistical and qualitative evaluation of multisources for hydrological suitability in flood-prone areas of Pakistan'. Journal of Hydrology 588(April):125117. https://doi.org/10.1016/j.jhydrol.2020.125117 (Elsevier)

Abro MI, Zhu D, Elahi E, Majidano AA, Solangi BK (2021) Hydrological simulation using multi-sources precipitation estimates in the Huaihe River Basin. Arabian Journal of Geosciences 2021(14):1–12. https://doi.org/10.1007/s12517-021-08254-1

Adediran GA (2015) Hydrological Forecasting with Radar and the Probability Distributed Hydrological Model (PDM). Dissertation.Com Boca Raton, Florida USA. https://doi.org/10.13140/RG.2.1.2556.7840

Ali RO, Chunju Z, Azam MI (2018) The effects of human activities, climatic conditions and land-use factors on water resources development in Huai river basin Northeast China. International Journal of Hydrology, 2(2):107–114. https://doi.org/10.15406/ijh.2018.02.00059

Amorim J da S, Viola MR, Junqueira R, de Oliveira VA, de Mello CR (2020) Evaluation of satellite precipitation products for hydrological modeling in the Brazilian cerrado biome. Water (Switzerland) 12(9). https://doi.org/10.3390/W12092571

Bengal W (2014) Application of sequential Mann-k\Kendall test for detection of approximate significant change point in surface air temperature for Kolkata weather observatory, west Bengal, India. International journal of current research 6(02):5319–5324

Bian GD, Du JK, Song MM, Xu YP, Xie SP, Zheng WL, Xu CY (2017) A procedure for quantifying runoff response to spatial and temporal changes of impervious surface in Qinhuai River basin of southeastern China. Catena 157(July 2016):268–278. https://doi.org/10.1016/j.catena.2017.05.023

Du J, Rui H, Zuo T, Li Q, Zheng D, Chen A, Xu CY (2013) Hydrological simulation by SWAT model with fixed and varied parameterization approaches under land use change. Water Resour Manage 27(8):2823–2838. https://doi.org/10.1007/s11269-013-0317-0

Fang GH et al (2015) Comparing bias correction methods in downscaling meteorological variables for a hydrologic impact study in an arid area in China, pp 2547–2559. https://doi.org/10.5194/hess-19-2547-2015

Gill PE et al (1981) Practical optimization, *Practical Optimization: Algorithms and Engineering Applications*, pp 1–669. https://doi.org/10.1007/978-0-387-71107-2

Gu H et al (2014) Impact of climate change on hydrological extremes in the Yangtze River impact of climate change on hydrological extremes in the Yangtze River Basin, China, (September). https://doi.org/10.1007/s00477-014-0957-5

Hao L, Sun G, Liu Y, Wan J, Qin M, Qian H, Chen J (2015) Urbanization dramatically altered the water balances of a paddy field-dominated basin in southern China. Hydrol Earth Syst Sci 19(7):3319–3331. https://doi.org/10.5194/hess-19-3319-2015

Huang A et al (2016) Journal of Geophysical Research : Atmospheres, pp 654–675. https://doi.org/10.1002/2016JD025456.Received

Kendall MG (1975) Rank Correlation Methods. 4th Edition, Charles Griffin, London

Mann HB (1945) Non-parametric test against trend. Econometrica 13:245-259. https://doi.org/10.2307/1907187

Maraun D (2016) Bias correcting climate change simulations - a critical review. Curr Clim Change Rep 2:211–220. https://doi.org/10.1007/s40641-016-0050-x

Mendez M, Maathuis B, Hein-Griggs D, Alvarado-Gamboa L-F (2020) Performance evaluation of bias correction methods for climate

change monthly precipitation projections. Water 12(482). https://doi.org/10.3390/w12020482
Moore RJ (1985) The probability-distributed principle and runoff production at point and basin scales. Hydrol Sci J 30(2):273–297. https://doi.org/10.1080/02626668509490989
Moore RJ (1999) 'Real-Time Flood Forecasting Systems: Perspectives and Prospects', Floods and Landslides: Integrated Risk Assessment, pp. 147–189. https://doi.org/10.1007/978-3-642-58609-5_11
Moore RJ (2007) The PDM rainfall-runoff model. Hydrol Earth Syst Sci 11(1):483–499. https://doi.org/10.5194/hess-11-483-2007
Nelder JA, Mead R (1965) A simplex method for function minimization. Comput J 7(4):308–313. https://doi.org/10.1093/comjnl/7.4.308
Niyongendako M et al (2020) Trend and variability analysis of rainfall and extreme temperatures in Burundi, 10(6):36–51. https://doi.org/10.9734/IJECC/2020/v10i630203
Nkunzimana A et al (2019) Spatiotemporal variation of rainfall and occurrence of extreme events over Burundi during 1960 to 2010. Arab J Geosci 12(5):176. https://doi.org/10.1007/s12517-019-4335-y
Oki T, Kanae S (2006) Global hydrological cycles and word water resources. Science 313(5790):1068–1072
O'Connor KM (1982) Derivation of discretely coincident forms of continuous linear time-invariant models using the transfer function approach. Journal of Hydrology 59(1–2):1–48. https://doi.org/10.1016/0022-1694(82)90002-6
Oleyiblo JO, Li Z (2010) Application of HEC-HMS for flood forecasting in Misai and Wan' an catchments in China. Water Sci Eng 3(1):14–22. https://doi.org/10.3882/j.issn.1674-2370.2010.01.002
Rica C (2020) Performance evaluation of bias correction methods for climate change monthly precipitation projections
Smith JM (1977) Mathematical modelling and digital simulation for engineers and scientists, Wiley, Chichester, UK. 332 pp
Sneyres R (1990) Technical note no. 143 on the statistical analysis of time series of observation. World Meteorological Organisation. Geneva, Switzerland
Song S, Xu YP, Yang L (2015) The effects of urbanization on catchment storage capacity – a conceptual model in plain catchment in Yangtz River Delta. Proceedings of the 14th International Conference on Environmental Science and Technology Rhodes, Greece, 3-5, September
Sridhar S, Raviraj A (2017) Statistical trend analysis of rainfall in Amaravathi River Basin using Mann-Kendall test. Curr World Environ 12(1):89–96. https://doi.org/10.12944/CWE.12.1.11
Tolika K (2019) Bias correction of climate model's precipitation using the copula method and its application in river basin simulation. https://doi.org/10.3390/w11030600
Vrac M, Noël T, Vautard R (2016) Bias correction of precipitation through singularity stochastic removal : because occurrences matter, (1), pp 5237–5258. https://doi.org/10.1002/2015JD024511. Received
Zhu D, Das S, Ren Q (2017) Hydrological appraisal of climate change impacts on the water resources of the Xijiang basin, South China. Water (Switzerland) 9(10):793. https://doi.org/10.3390/w9100793
Zhu D et al (2020) Hydrological evaluation of hourly merged satellite–station precipitation product in the mountainous basin of China using a distributed hydrological model. Meteorol Appl 27(2):1–16. https://doi.org/10.1002/met.1909

Authors and Affiliations

Basile A. Akpovi[1] · Dehua Zhu[2] · Muhammad Ilyas Abro[2] · Agnidé Emmanuel Lawin[3] · Mendela Houngnibo[4] · Joseph Bessou[4]

Dehua Zhu
d.zhu@nuist.edu.cn

Agnidé Emmanuel Lawin
ewaari@yahoo.fr

Mendela Houngnibo
hmandelahmadiba@yahoo.fr

Joseph Bessou
bessoujoseph68@gmail.com

[1] Agence Météo-Bénin, P.O. Box 01 BP 379, Cotonou, Benin

[2] School of Hydrology and Water Resources, Nanjing University of Information Science and Technology, No. 219, Ningliu Road, Nanjing, Jiangsu, China

[3] Laboratory of Applied Hydrology, National Institute of Water, University of Abomey-Calavi, P.O. Box 2041, Calavi, Benin

[4] Agence Météo-Bénin, P.O. Box 01 BP : 379 Cotonou, Benin, Pob 11011, Cotonou, Benin